Efficacy and Self-Similarity of SARS-CoV-2 Thermal Decontamination

Te Faye Yap,[1,†] Jason C. Hsu,[2,†] Zhen Liu,[1] Kempaiah Rayavara,[2] Vivian Tat,[2] Chien-Te K. Tseng,[2,3] and Daniel J. Preston[1,*]

[1]Department of Mechanical Engineering, George R. Brown School of Engineering, Rice University; 6100 Main St., Houston, TX 77005, USA.

[2]Department of Microbiology and Immunology, University of Texas Medical Branch; 301 University Blvd., Galveston, TX 77555, USA.

[3]Center for Biodefense and Emerging Disease, Galveston National Laboratory, University of Texas Medical Branch; 301 University Blvd., Galveston, TX 77555, USA.

DOI: https://doi.org/10.1016/j.jhazmat.2021.127709

Highlights

- Empirical data alone does not explain the thermal virus inactivation reaction.
- This work develops and validates a modeling framework based on reaction kinetics.
- The results reveal self-similar behavior during inactivation of coronaviruses.
- Heating surgical masks to 70 °C for 5 minutes inactivates > 99.9% of SARS-CoV-2.
- XPS, SEM, and contact angle show no physical or chemical degradation of the masks.

Abstract

Dry heat decontamination has been shown to effectively inactivate viruses without compromising the integrity of delicate personal protective equipment (PPE), allowing safe reuse and helping to alleviate shortages of PPE that have arisen due to COVID-19. Unfortunately, current thermal decontamination guidelines rely on empirical data which are often sparse, limited to a specific virus, and unable to provide fundamental insight into the underlying inactivation reaction. In this work, we experimentally quantified dry heat decontamination of SARS-CoV-2 on disposable masks and validated a model that treats the inactivation reaction as thermal degradation of macromolecules. Furthermore, upon nondimensionalization, all of the experimental data collapse onto a unified curve, revealing that the thermally driven decontamination process exhibits self-similar behavior. Our results show that heating surgical masks to 70 °C for 5 minutes inactivates over 99.9% of SARS-CoV-2. We also characterized the chemical and physical properties of disposable masks after heat treatment and did not observe degradation. The model presented in this work enables extrapolation of results beyond specific temperatures to provide guidelines for safe PPE decontamination. The modeling framework and self-similar behavior are expected to extend to most viruses—including yet-unencountered novel viruses—while accounting for a range of environmental conditions.

Keywords: COVID-19; Dry heat decontamination; Personal protective equipment; Arrhenius equation; Reaction rate law.

1. Introduction

The COVID-19 pandemic has challenged the global healthcare system and exposed frontline healthcare workers to an unacceptable level of risk. The relatively high reproduction number of SARS-CoV-2 (Sanche et al., 2020; Zhu and Chen, 2020) has resulted in a surge in hospitalization rates and, in turn, a shortage of personal protective equipment (PPE); in many instances, disposable masks had to be reused (Kolata, 2020; Rowan and Laffey, 2020). Despite the rollout of vaccines, PPE shortages may continue to occur in countries with a relatively low Human Development Index for years to come, and this risk is elevated by the rise of dangerous variants (Callaway, 2021; Mahase, 2021; Samarasekera, 2021). Various decontamination methods—including UV irradiation, steam sterilization, and chemical disinfectants—have been implemented, but these methods suffer from several drawbacks, namely: (i) UV irradiation only inactivates viruses that are illuminated and is ineffective within folds and crevices commonly present in fabric-based PPE (Cramer et al., 2020; Jinia et al., 2020; Raeiszadeh and Adeli, 2020); (ii) steam or moist heat sterilization relies on water vapor at high temperatures and pressures to sterilize equipment at a relative humidity of 100%, which can compromise the filtration efficiency of masks (Campos et al., 2020); and (iii) chemical disinfectants leave harmful chemical residues within the porous structures of some PPE and may degrade the material (Jinia et al., 2020; Viscusi et al., 2009).

Dry heat decontamination is performed at elevated temperatures, but at relative humidities less than 100%, by heating the air surrounding the equipment to be decontaminated. The high elevated temperatures applied during typical dry heat decontamination have been shown to degrade polymer-based PPE (Viscusi et al., 2007). However, when performed at lower elevated

44 temperatures (albeit over longer periods of time), dry heat decontamination represents a
45 promising alternative to other approaches and has been shown to effectively inactivate viruses
46 while retaining the efficacy and integrity of disposable masks (Liao et al., 2020; Oh et al., 2020).
47 Moreover, appliances for dry heat decontamination are attainable in most households (*e.g.*, home
48 ovens or rice cookers). Oh *et al.* demonstrated the feasibility of dry heat decontamination of N95
49 respirators using a household electric cooker and found that the filtration performance and fit of
50 the respirators were not compromised after 20 cycles of heat treatment (Oh et al., 2020). Other
51 experiments on the thermal decontamination of SARS-CoV-2 have been performed on various
52 surfaces across a range of temperatures, providing empirical guidelines for PPE decontamination
53 (Campos et al., 2020; Chin et al., 2020; van Doremalen et al., 2020). These experimental results
54 are promising, but they are often sparse, only reflect virus inactivation at specific temperatures,
55 and do not provide a fundamental understanding of the effect of temperature on the rate of virus
56 inactivation. On the other hand, analytical models which treat viruses as macromolecules
57 undergoing thermal degradation have been used to describe the relationship between temperature
58 and virus inactivation (Yap et al., 2020), but these models have not been validated with
59 experimental results. A reliable model would reduce the number of experiments required to
60 capture the thermal inactivation behavior of a specific virus while also providing comprehensive
61 thermal decontamination guidelines. In this work, we experimentally quantified thermal
62 decontamination of surgical masks inoculated with SARS-CoV-2, and, using the results, we
63 validated a model of the virus inactivation reaction that can predict the lifetime of SARS-CoV-2
64 as a continuous function of temperature (Fig. 1A).

2. Materials and Methods

2.1 SARS-CoV-2 thermal inactivation experiments

We conducted dry heat decontamination experiments at 25 °C, 40 °C, 55 °C, and 70 °C at a relative humidity within the range of 48 – 55% in a biosafety cabinet. We chose 25 °C to correspond to standard ambient conditions. We chose 70 °C as our maximum temperature for three reasons: (i) it is the lowest setting in typical home ovens; (ii) it has been suggested as a dry heat decontamination temperature by the FDA; and (iii) 70 °C is a typical temperature used for pasteurization (Iijima et al., 2001; Islam and Johnston, 2006; Xiang et al., 2020; Zha et al., 2021). Surgical masks (Canuxi Disposable Face Masks, SKU 810484847) were cut into 5 cm by 5 cm samples and inoculated with SARS-CoV-2 virus stock. The samples were placed on an oven pan and heated in a home-use oven (Brentwood, TS-345R) at the specified decontamination temperatures. The countertop oven and stainless-steel oven pan were preheated to the desired inactivation temperature and monitored with a digital thermometer (Fisherbrand, 14-648-46). The temperature dial settings for the three temperatures tested in this study were measured and determined beforehand in a BSC in a BSL-2 laboratory in order to replicate potential experimental conditions in a low-risk environment. Then, either a 1 mL droplet of the low-titer virus culture (for the 25 ℃, 40 ℃, and 55 ℃ experiments) or a 100 µL droplet of the high-titer virus culture (for the 70 ℃ experiment) was pipetted onto the outer layer of each surgical mask sample and left at room temperature (~25 ℃) while the oven was preheating. When the oven temperature stabilized within ± 3 ℃ of the desired temperature for 30 minutes, the oven pan was taken out and each inoculated mask sample was carefully transferred (taking approximately five seconds per mask sample) onto the oven pan with the viral inoculum side facing upwards and placed back inside the oven for dry heat treatment. Each mask piece was removed from the oven

once the desired time point was reached and immediately soaked in 10 mL of 2% FBS-MEM virus transfer medium in a 50 mL conical centrifuge tube for at least 30 minutes to recover the virus.

After the 30 minutes elapsed, the recovered virus medium was titrated *via* a standard $TCID_{50}$ assay procedure (Algaissi et al., 2018; Hashem et al., 2019; Tao et al., 2015) in Vero-E6 cells. We performed 1:10 serial dilutions of the virus samples using 50 µL as the starting titer until the theoretical dilution was equal to 1 $TCID_{50}$/mL (*i.e.*, 0 log $TCID_{50}$/mL); because the highest viral stock titer was 1×10^7 $TCID_{50}$/mL, of which we used only 100 µL to reach a theoretical maximum titer of 1×10^6 $TCID_{50}$/mL, we performed serial dilutions from 10^{-1} to 10^{-6}. We then aliquoted 100 µL from each dilution to a well on a 96-well microtiter plate of fully confluent Vero-E6 cells, with four wells per dilution and four samples per plate. We incubated the plates infected with the virus at 37 °C for three days, after which we observed each plate for cytopathic effects (CPE) and counted the number of "dead" wells showing CPE in each dilution for each sample. Finally, we estimated the number of viable virus particles using the Reed and Muench method for $TCID_{50}$ quantification (Reed and Muench, 1938).

Each of the four time points at each temperature was performed in triplicate for a total of twelve samples for each temperature, and forty-eight samples in total across all temperatures. We used a 500 µL vial of the virus stock held at room temperature as a positive control and starting titer quantification, denoted by the virus titer at 0 minutes in Fig. 1B. For the room temperature series of experiments, we immediately titrated the 500 µL virus stock vial as the positive control and starting titer.

2.2 Cells, media, and viruses

The Vero-E6 cells (CRL-1580, American Type Culture Collection) were grown in Eagle's Minimal Essential Medium (MEM) (Corning, 10-010-CV) supplemented with 10% fetal bovine serum (FBS) (GIBCO, 10437-028), 2% L-Glutamine (GIBCO, 25030-164), and 1% Penicillin-Streptomycin (GIBCO, 15140-122), designated 10-MEM. A cell culture medium with a similar composition to 10-MEM, but supplemented with 2% FBS instead of 10% FBS, was designated as 2-MEM and used to culture and transfer the virus. The 2-MEM virus culture medium represents a realistic surrogate for human saliva, through which SARS-CoV-2 is primarily transmitted in the form of aerosolized droplets, in terms of protein concentration, and in fact contains a higher protein concentration (at least 2% total protein per milliliter of medium) than saliva, which has been estimated to contain about 0.3% total protein in a typical 1-2 mL sample (Lagerlof and Dawes, 1984; Schipper et al., 2007; Woo et al., 2010).

The USA-WA1/2020 strain of SARS-CoV-2, provided to us by Dr. Natalie Thornburg at the Centers for Disease Control (CDC), Atlanta, GA, through the World Reference Center for Emerging Viruses and Arboviruses (WRCEVA), was used throughout this study. The original stock of SARS-CoV-2 was cultured in 2-MEM and passaged two more times in Vero-E6 cells to generate the working viral stocks, which were stored at -80 ℃. The two working viral stocks used throughout this study were titrated at either 1×10^5 $TCID_{50}$/mL or 1×10^7 $TCID_{50}$/mL by the standard $TCID_{50}$ assay in Vero-E6 cells as previously described (Algaissi et al., 2018; Hashem et al., 2019; Tao et al., 2015), designated as the “low-titer” and “high-titer” stocks, respectively. Both of these experimental inoculating titers are greater than the average amount of SARS-CoV-2 virions detected in saliva of COVID-19 patients as quantified using quantitative reverse-

transcriptase polymerase chain reaction (qRT-PCR), which does not discriminate between replicative and non-replicative viral particles (Ceron et al., 2020). All experiments involving infectious SARS-CoV-2 were conducted at Galveston National Laboratory (GNL) in the biosafety cabinet (BSC) in an approved biosafety level (BSL) laboratory (*i.e.*, BSL-3) following all approved notification-of-use and safety protocols.

2.3 Physical morphology and chemical composition of surgical masks after heating

We visualized the physical structure of the meltblown filter layer (*i.e.*, the middle layer of a typical three-layer surgical mask responsible for filtration) before and after heat treatment at 70 °C for 30 minutes, 125 °C for 30 minutes, 150 °C for 10 minutes, 155 °C for 2 minutes, and 160 °C for 2 minutes using scanning electron microscopy. The filter layer was first sputtered with a 10-nm-thick coating of Au to improve the conductivity of the surface. A field emission scanning electron microscope (FEI Quanta 400 ESEM FEG) was then used to take images with the secondary electron detector at an accelerating voltage of 10 kV.

The chemical composition of the meltblown filter layer before and after heat treatment was characterized using X-ray photoelectron spectroscopy (XPS). The XPS measurements were carried out using a conventional Al Kα (1486.6 eV) X-ray source. A survey scan was conducted to determine the elements present on the surface and detailed scans show the relative peak magnitudes of carbon and oxygen.

We characterized the wettability of the surgical mask hydrophobic outer layer before and after heating with a contact angle goniometer using the sessile drop technique. The advancing and

157 receding water contact angles were measured at 10 different locations on the surgical mask. The
158 goniometer utilized a 5.0 MP, 35 FPS camera (CM3-U3-50S5C-CS Chameleon3, FLIR)
159 equipped with a 0.25x telecentric lens (55-349 GoldTL, Edmund Optics), and the liquid droplet
160 was generated with syringe pump (PHD 2000, Harvard Apparatus) using deionized water at
161 room temperature and pressure. The values of the advancing and receding contact angles were
162 determined by processing the captured images with custom-made Matlab scripts (using
163 polynomial curve fitting to characterize the droplet profile and solid surface).
164

165 ## 3. Results and discussion

166 ### 3.1 Experimental validation of the reaction kinetics model

167 We conducted dry heat decontamination experiments on surgical masks inoculated with SARS-
168 CoV-2 virus culture at the temperatures and durations shown in Fig. 1B and at a relative
169 humidity (RH) within the range of 48 – 55% at room temperature. As the temperature for a fixed
170 volume of air in the oven increases, the RH inside the oven decreases. Based on the initial vapor
171 density corresponding to a RH of 50% at room temperature (25 °C), we estimate RH values of
172 23%, 11%, and 6% at 40 °C, 55 °C, and 70 °C, respectively (the steps to determine RH at
173 elevated temperature are included in the Supplementary Material). Our experimental results and
174 model indicate that 70 °C is sufficient to decontaminate surgical masks in less than 5 minutes
175 according to the FDA-specified 3-log reduction in viable virions (CDC, 2008; FDA, 2020; Oral
176 et al., 2020). We applied our experimental results to validate a model of the reaction kinetics
177 based on the rate law for a first-order reaction and the Arrhenius equation (Yap et al., 2020). This
178 model (Eq. 1) describes the inactivation reaction as thermal degradation of the proteins that
179 comprise each virion (Qiao and De La Cruz, 2020) to predict the time required to achieve an *n*-

log reduction (*i.e.*, the ratio of final viable concentration of virus to its initial concentration in terms of order of magnitude, where $[C]/[C_0] = 10^{-n}$).

$$t_{n-log} = -\frac{1}{A} e^{\frac{Ea}{RT}} \ln(10^{-n}) \quad \text{(Eq. 1)}$$

The activation energy, E_a, and natural log of the frequency factor, $\ln(A)$, were determined for SARS-CoV-2 on the surgical masks tested in this work using a linear regression approach described in prior work (Yap et al., 2020) and detailed in the Supplementary Material.

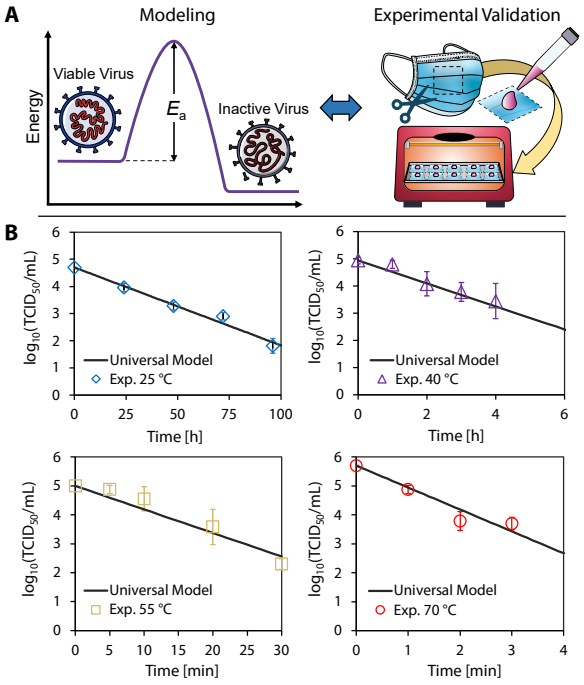

Figure 1. *Validation of model with experimental results. (A) The universal model combines the rate law and the Arrhenius equation to determine the activation energy required to inactivate a specific virus. Surgical mask samples were inoculated with SARS-CoV-2 and exposed to 25 °C, 40 °C, 55 °C, and 70 °C dry heat in an oven. (B) The samples were assayed at different times; the plots show the corresponding $\log_{10}$ reduction in viable virus concentration at a given temperature. Each experimental data point was assayed in triplicate, and error bars correspond to the standard deviation among the triplicate measurements. Our universal model based on the reaction kinetics was plotted and exhibited close agreement with experimental data.*

The inactivation behavior of SARS-CoV-2 agrees with the Meyer-Neldel rule for entropy-enthalpy compensation exhibited by other coronaviruses (Fig. S3). Furthermore, the E_a and ln(A) values for SARS-CoV-2 determined in this work deviate by only 2.5% and 1.5%, respectively, from the values determined in prior work based on a data-driven analysis (*i.e.*, without original experimental results) across a range of fomites (Table S1).

This universal model (Eq. 1) is plotted in Fig. 1B for the four temperatures studied in this work; the close agreement with the experimental data serves to validate the modeling framework. The data shown here also agree with prior experimental results for room temperature inactivation of SARS-CoV-2 on surgical masks, for which a 3-log reduction requires approximately 100 hours (Chin et al., 2020). From experimental results obtained over 25 °C–70 °C, the decontamination time of SARS-CoV-2 on surgical face masks ranges from up to 100 hours to as little as 5 minutes, spanning more than three orders of magnitude and highlighting the exponential dependence of virus inactivation time on temperature as shown in Eq. 1. We note that earlier reports have suggested the possibility of multiple inactivation reaction pathways at different temperatures (Laude, 1981); the data shown here follow a single first-order reaction pathway.

3.2 Self-similarity of virus thermal inactivation

We went on to show that the thermal inactivation process exhibits self-similarity. Self-similar behavior has been identified in phenomena ranging from fluid flows (Aagesen et al., 2010; Day et al., 1998) to complex networks (Ganan-Calvo and Hernandez Ramos, 2020; Song and Havlin, 2005) in prior work, but had not yet been reported for viruses.

To nondimensionalize the relevant parameters, we first define a thermal decontamination timescale, τ_{decon}, in Eq. 2:

$$\tau_{decon} = \frac{\ln(10)}{A} e^{\frac{E_a}{RT}} \quad \text{(Eq. 2)}$$

Nondimensionalizing time with respect to the thermal decontamination timescale yields the dimensionless time, $t^* = t/\tau_{decon}$. The concentration is then nondimensionalized by dividing by the initial concentration, $[C]^* = [C]/[C_0]$.

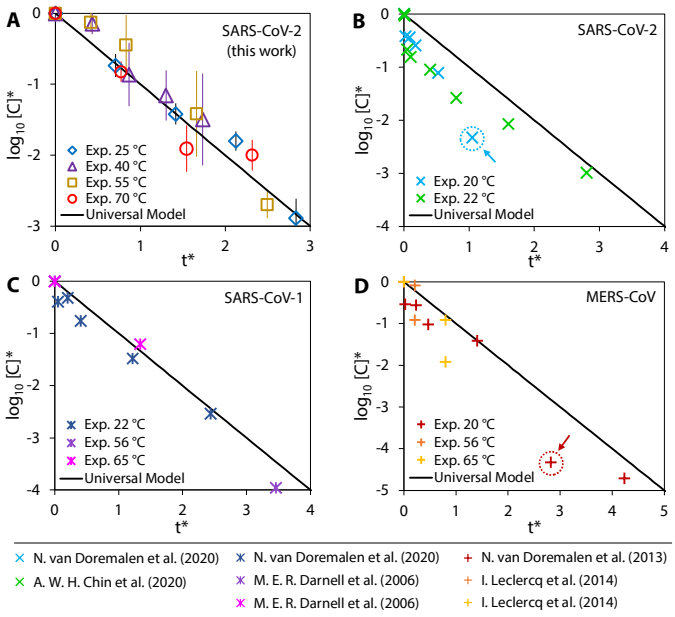

Figure 2. Self-similar behavior of virus inactivation. *The nondimensionalized experimental data for thermal inactivation of SARS-CoV-2 in this work collapse onto a single universal model curve* ***(A)****. Experimental data from prior work on the thermal inactivation of SARS-CoV-2* ***(B)****, SARS-CoV-1* ***(C)****, and MERS-CoV* ***(D)*** *were nondimensionalized and compared to our universal model. The comparison reveals that the thermal inactivation processes of all the coronaviruses considered here exhibit the same form of self-similar behavior.*

Plotting the nondimensionalized experimental data, we show that the data points collapse onto a single universal model prediction (Fig. 2A) for which $n = -t^*$, indicating that the thermal inactivation process exhibits fundamental self-similarity and the order of viral reduction, n, is directly proportional to t^*. This new understanding will allow application of our results across a wide range of temperatures beyond the four specific temperatures studied here.

From the nondimensionalized plot, we are also able to identify the experimental temperature and duration that achieves a desired n-log reduction. We compared our universal model prediction to prior experimental work on SARS-CoV-2 (Chin et al., 2020; van Doremalen et al., 2020), SARS-CoV-1 (Darnell and Taylor, 2006; van Doremalen et al., 2020), and MERS-CoV (Leclercq et al., 2014; van Doremalen et al., 2013) and found that, upon nondimensionalizing the data from these reports, the inactivation trend was also described by our model and exhibited self-similarity (Fig. 2B – D). These three coronaviruses were chosen because they are highly pathogenic human coronaviruses and the results could be relevant to further understand their inactivation behavior (Cevik et al., 2021; Zhu et al., 2020).The inactivation results reported in literature for these three coronaviruses generally follow the self-similar trend with the exception of two outliers indicated with arrows in Fig. 2B and D; outliers were determined using a standard procedure based on the standard deviation of the residuals (Illowsky and Dean, 2021). The deviation of these two outliers from the universal model prediction may indicate potential experimental error in the results, suggesting that researchers working on the thermal inactivation of viruses can use this model as a benchmark to compare against experiments in future work.

3.3 Surgical masks before and after dry heat decontamination

To complement the underlying concept of thermal inactivation of viruses and enable practical use, prior work has focused on studying the filtration performance and fit test of disposable masks after dry heat decontamination. Oh *et al.* performed filtration performance, pressure drop, and quantitative fit testing after dry heat decontamination at 100 °C and 5% RH for 50 minutes. After 20 cycles of decontamination, they found that the particle filtration efficiency was 97% (above the minimum filtration efficiency requirement of 95% for N95 respirators), with no significant changes in pressure drop (Oh et al., 2020). The average fit factor was 139, well above the passing score of 100. Another study by Xiang *et al*. conducted dry heat decontamination on N95 respirators and surgical masks at 70 °C for 1, 2, and 3 hours and showed that filtration efficiencies remained greater than 96% (Xiang et al., 2020). Additional work studying the electrostatic charge on mask filter layers, which is partially responsible for filtering of small particles by electrostatic adsorption, found that dry heat treatment at low humidities (< 30% RH) and low temperatures (< 100 °C) for 20 cycles did not decay the electrostatic charges and the efficiency of the filters (Campos et al., 2020; Liao et al., 2020). Fit tests conducted by Zha et al. after one cycle of dry heat decontamination at 75 °C for 30 minutes show that 93% of N95 respirators passed the fit test if the respirator was donned and doffed less than 5 times prior to dry heat decontamination (Zha et al., 2021).

The results presented in the literature indicate that dry heat decontamination at 70 °C (the maximum temperature applied in this work) for 5 minutes will not degrade the filtration efficiency of masks; to further supplement prior results, we provide additional characterization of the effect of dry heat treatment on the material properties of the mask layers at 70 °C for 30

minutes (more than six times the duration required for effective decontamination) to provide fundamental insight into the micro- and nanoscale morphology and chemical composition of disposable masks and N95 respirators (*i.e.,* masks made from nonwoven polypropylene fibers). We characterized the chemical composition of the meltblown filter layer (*i.e.*, the middle layer of a typical three-layer surgical mask responsible for filtration) using X-ray photoelectron spectroscopy (XPS). The XPS survey spectrum as well as detailed O 1s and C 1s spectra of the unheated and heated filters are shown in Fig. 3A. Heat treatment at 70 °C for 30 minutes did not alter the elemental composition, nor did it result in any oxidation as evidenced by the detailed O 1s spectra. The detailed C 1s spectra indicate that some sp^2 carbon converted to sp^3 during the heating process, which suggests strengthening of the material in an annealing-like process and a potential increase in surface hydrophobicity (Paul et al., 2008).

We visualized the physical morphology of the meltblown filter layer of the surgical mask before and after heat treatment using electron microscopy (Fig. 3B). The images in Fig. 3B show that there are no apparent physical changes in the microscale morphology or structure of the fibers. In contrast, we also heated surgical masks to high temperatures typical for dry heat decontamination (~160 °C) and observed significant degradation of the meltblown filter layer (Fig. S5), illustrating the sensitivity of the material properties and physical morphologies of the meltblown filter layer to temperature, especially when operating close to the melting point of the polymer.

To ensure that the functionality of the hydrophobic outer layer of the 3-ply surgical mask (*i.e.*, the outermost layer relative to the wearer) was not altered after dry heat decontamination, water contact angle measurements were taken on the outer layer before and after heat treatment at

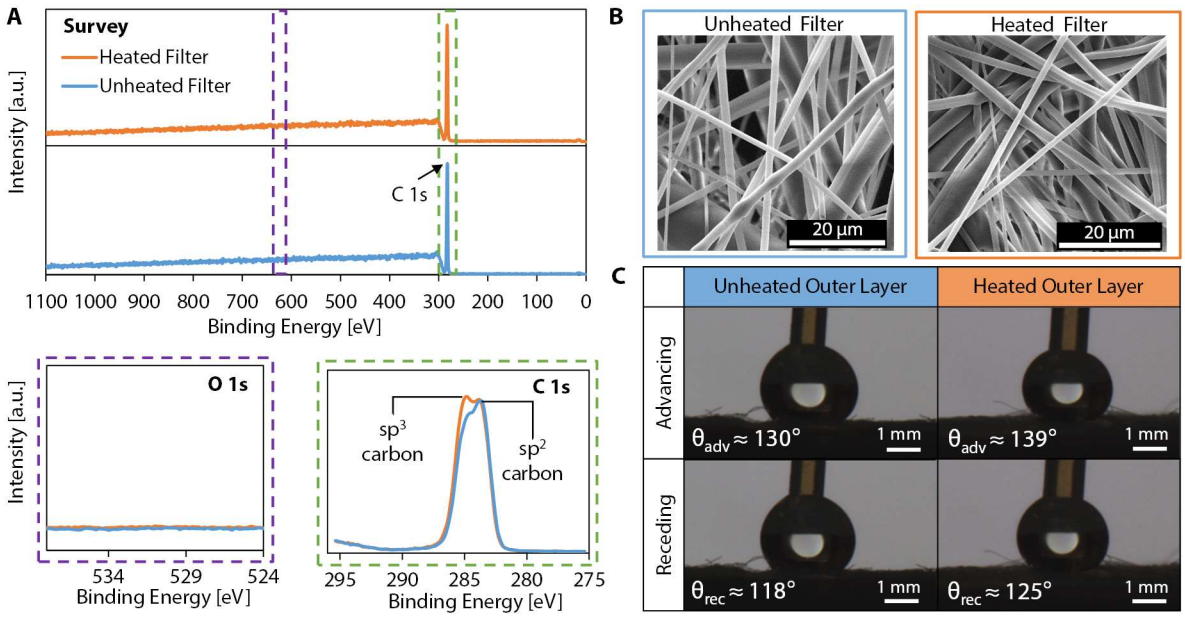

Figure 3. Chemical composition and physical morphology of surgical mask before and after heat treatment. *The chemical morphology of the disposable mask before and after heat treatment was observed. (**A**) Survey XPS spectra and detailed O 1s and C 1s spectra were obtained for both the unheated and heated mask filter layers (all vertical scalings are identical). The survey spectra show the same elemental composition for unheated and heated mask filter layers. No oxidation is observed after heat treatment, as evidenced by the detailed O 1s spectra. The detailed C 1s spectra indicate that some sp^2 carbon was converted to sp^3 carbon during heating. (**B**) Scanning electron microscope (SEM) images show the physical morphology of the meltblown filter layer before and after application of heat treatment at 70 °C for a period of 30 minutes. (**C**) Representative images of a droplet advancing and receding on the hydrophobic outer layer of the 3-ply disposable mask and the average contact angle measurements before and after heat treatment at 70 °C for 30 minutes.*

70 °C for 30 minutes; we found that the heat treatment did not significantly change the surface wettability of the hydrophobic mask layer (Fig. 3C). We observed small increases in the advancing and receding contact angles (average values shown on Fig. 3C) on the outer layer after heat treatment, likely due to the conversion of sp^2 carbon to sp^3 carbon during the heating process as observed on the meltblown filter layer. These results indicate that dry heat

317 decontamination, in addition to effectively inactivating SARS-CoV-2 in short times and at
318 temperatures available in most home devices, is also appropriate for delicate PPE, including
319 masks.
320
321 **3.4 Limitations of the universal model**
322 We note that the model presented here focuses solely on the effect of temperature and does not
323 consider relative humidity, which has been shown to affect virus lifetime (Chan et al., 2011; Lin
324 and Marr, 2020); however, recent work suggests that relative humidity may be integrated into a
325 reaction-rate-based model, such as the one presented in this work (Morris et al., 2020). Different
326 fomites are also known to alter virus lifetime by up to an order of magnitude (Bayarri et al.,
327 2021; Imani et al., 2020; van Doremalen et al., 2020), and incorporation of fomite material in the
328 model, interpreted as a catalyst (*i.e.*, by modifying E_a and $\ln(A)$), may allow this modeling
329 framework to accurately predict virus lifetimes across a range of fomites (Roduner, 2014). We
330 also note that the salt and protein concentrations in the virus culture medium could affect the
331 virus' resistance to heat; in future work, we could use our current work as a baseline to study the
332 effects of salt and protein concentration on the temperature-dependent rate of inactivation. The
333 model is limited in terms of extrapolation to higher temperatures, for which alternate reaction
334 pathways may dominate. Finally, we note that the samples were assumed to have a constant
335 temperature during decontamination due to the short transient heating periods (at most, ~10% of
336 the total heating duration for the shortest decontamination duration at 70 °C as detailed in the
337 Supplementary Material); however, time-varying temperature profiles could be accounted for by
338 adjusting the model for objects with a larger thermal mass that exhibit longer time-dependent
339 temperatures as they equilibrate with their surroundings (Yap et al., 2021).

4. Conclusions

This work validates a model based on reaction kinetics to predict the time required for SARS-CoV-2 decontamination, providing much-needed guidelines to allow safe reuse of PPE. With this modeling framework, the number of experiments required to characterize the effects of temperature for a specific virus can be greatly reduced, and early dissemination of decontamination guidelines for yet-unencountered novel viruses will become attainable. In addition to temperature, the decontamination timescale is a function of the activation energy and the frequency factor; adjusting E_a and $\ln(A)$ would allow for the thermal inactivation behavior of most viruses to collapse onto the single unified model curve presented in this work. Extension of the model to include environmental conditions such as relative humidity and fomite material could ultimately provide a pathway toward a comprehensive model of virus inactivation that applies to all viruses, with the self-similar behavior of the thermal inactivation process applied as a metric to understand the requirements for safe and effective decontamination.

CRediT authorship contribution statement

Te Faye Yap: Conceptualization, Formal Analysis, Visualization, Methodology, Writing – original draft and review & editing. Jason Hsu: Investigation, Methodology, Writing – review & editing. Zhen Liu: Methodology, Visualization, Writing – review & editing. Kempaiah Rayavara: Investigation, Writing – review & editing. Vivian Tat – Investigation, Writing – review & editing. Chien-Te K. Tseng – Supervision, Funding Acquisition, Writing – review & editing. Daniel J. Preston: Supervision, Conceptualization, Methodology, Funding Acquisition, Writing – original draft and review & editing.

Declaration of interests

All authors declare no competing interests.

Acknowledgments

This work was supported by the National Science Foundation under grants CBET-2030023 and CBET-2030117 with Dr. Ying Sun as program director. This work was conducted in part using resources provided by the Shared Equipment Authority at Rice University. We would like to acknowledge Dr. Aleksandra Drelich for technical assistance provided in interpreting preliminary results and constructive suggestions during the planning of this project.

Appendix A. Supplementary Material

Supplementary data associated with this article can be found in the online version.

Graphical abstract

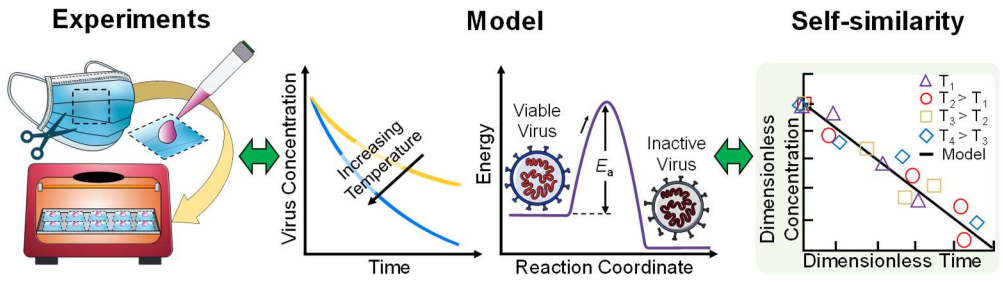

References

Aagesen, L.K., Johnson, A.E., Fife, J.L., Voorhees, P.W., Miksis, M.J., Poulsen, S.O., Lauridsen, E.M., Marone, F., Stampanoni, M., 2010. Universality and self-similarity in pinch-off of rods by bulk diffusion. Nat. Phys. 6, 796–800.

https://doi.org/10.1038/nphys1737

Algaissi, A., Agrawal, A.S., Han, S., Peng, B.-H., Luo, C., Li, F., Chan, T.-S., Couch, R.B., Tseng, C.-T.K., 2018. Elevated Human Dipeptidyl Peptidase 4 Expression Reduces the Susceptibility of hDPP4 Transgenic Mice to Middle East Respiratory Syndrome Coronavirus Infection and Disease. J. Infect. Dis. 219, 829–835. https://doi.org/10.1093/infdis/jiy574

Bayarri, B., Cruz-Alcalde, A., López-Vinent, N., Micó, M.M., Sans, C., 2021. Can ozone inactivate SARS-CoV-2? A review of mechanisms and performance on viruses. J. Hazard. Mater. 415. https://doi.org/10.1016/j.jhazmat.2021.125658

Callaway, E., 2021. Delta Coronavirus Variant : Scientists Brace for Impact. Nature 595, 17–18. https://doi.org/10.1038/d41586-021-01696-3

Campos, R.K., Jin, J., Rafael, G.H., Zhao, M., Liao, L., Simmons, G., Chu, S., Weaver, S.C., Chiu, W., Cui, Y., 2020. Decontamination of SARS-CoV-2 and other RNA viruses from N95 level meltblown polypropylene fabric using heat under different humidities. ACS Nano 14, 14017−14025. https://doi.org/10.1021/acsnano.0c06565

CDC, 2008. Disinfection of Healthcare Equipment. https://www.cdc.gov/infectioncontrol/guidelines/disinfection/healthcare-equipment.html

Ceron, J.J., Lamy, E., Martinez-Subiela, S., Lopez-Jornet, P., Capela E Silva, F., Eckersall, P.D., Tvarijonaviciute, A., 2020. Use of Saliva for Diagnosis and Monitoring the SARS-CoV-2: A General Perspective. J. Clin. Med. 9, 1491. https://doi.org/10.3390/jcm9051491

Cevik, M., Tate, M., Lloyd, O., Maraolo, A.E., Schafers, J., Ho, A., 2021. SARS-CoV-2, SARS-CoV, and MERS-CoV viral load dynamics, duration of viral shedding, and infectiousness: a systematic review and meta-analysis. The Lancet Microbe 2, e13–e22.

https://doi.org/10.1016/S2666-5247(20)30172-5

Chan, K.H., Peiris, J.S.M., Lam, S.Y., Poon, L.L.M., Yuen, K.Y., Seto, W.H., 2011. The effects of temperature and relative humidity on the viability of the SARS coronavirus. Adv. Virol. 2011, 1–7. https://doi.org/10.1155/2011/734690

Chin, A.W.H., Chu, J.T.S., Perera, M.R.A., Hui, K.P.Y., Yen, H.-L., Chan, M.C.W., Peiris, M., Poon, L.L.M., 2020. Stability of SARS-CoV-2 in different environmental conditions. The Lancet Microbe 1, e10. https://doi.org/10.1016/S2666-5247(20)30003-3

Cramer, A., Tian, E., Yu, S.H., Galanek, M., Lamere, E., Li, J., Gupta, R., Short, M.P., 2020. Disposable N95 Masks Pass Qualitative Fit-Test But Have Decreased Filtration Efficiency after Cobalt-60 Gamma Irradiation. medRxiv. https://doi.org/10.1101/2020.03.28.20043471

Darnell, M.E.R., Taylor, D.R., 2006. Evaluation of inactivation methods for severe acute respiratory syndrome coronavirus in noncellular blood products. Transfusion 46, 1770–1777. https://doi.org/10.1111/j.1537-2995.2006.00976.x

Day, R.F., Hinch, E.J., Lister, J.R., 1998. Self-similar capillary pinchoff of an inviscid fluid. Phys. Rev. Lett. 80, 704–707. https://doi.org/10.1103/PhysRevLett.80.704

FDA, 2020. Investigating Decontamination and Reuse of Respirators in Public Health Emergencies.

Ganan-Calvo, A.M., Hernandez Ramos, J.A., 2020. The fractal time growth of COVID-19 pandemic : an accurate self-similar model , and urgent conclusions. arXiv 1–13.

Hashem, A.M., Algaissi, A., Agrawal, A.S., Al-Amri, S.S., Alhabbab, R.Y., Sohrab, S.S., S Almasoud, A., Alharbi, N.K., Peng, B.-H., Russell, M., Li, X., Tseng, C.-T.K., 2019. A Highly Immunogenic, Protective, and Safe Adenovirus-Based Vaccine Expressing Middle East Respiratory Syndrome Coronavirus S1-CD40L Fusion Protein in a Transgenic Human

Dipeptidyl Peptidase 4 Mouse Model. J. Infect. Dis. 220, 1558–1567. https://doi.org/10.1093/infdis/jiz137

Iijima, Y., Karama, M., Oundo, J.O., Honda, T., 2001. Prevention of bacterial diarrhea by pasteurization of drinking water in Kenya. Microbiol. Immunol. 45, 413–416. https://doi.org/10.1111/j.1348-0421.2001.tb02639.x

Illowsky, B., Dean, S., 2021. Outliers. https://stats.libretexts.org/@go/page/802 (accessed 10.7.21).

Imani, S.M., Ladouceur, L., Marshall, T., Maclachlan, R., Soleymani, L., Didar, T.F., 2020. Antimicrobial Nanomaterials and Coatings : Current Mechanisms and Future Perspectives to Control the Spread of Viruses Including SARS-CoV-2. ACS Nano 14, 12341−12369. https://doi.org/10.1021/acsnano.0c05937

Islam, M.F., Johnston, R.B., 2006. Household pasteurization of drinking-water: The Chulli water-treatment system. J. Heal. Popul. Nutr. 24, 356–362. https://doi.org/10.3329/jhpn.v24i3.721

Jinia, A.J., Sunbul, N.B., Meert, C.A., Miller, C.A., Clarke, S.D., Kearfott, K.J., Matuszak, M.M., Matuszak, M.M., Pozzi, S.A., 2020. Review of Sterilization Techniques for Medical and Personal Protective Equipment Contaminated with SARS-CoV-2. IEEE Access 8, 111347–111354. https://doi.org/10.1109/ACCESS.2020.3002886

Kolata, G., 2020. As Coronavirus Looms, Mask Shortage Gives Rise to Promising Approach. New York Times.

Lagerlof, F., Dawes, C., 1984. The Volume of Saliva in the Mouth Before and After Swallowing. J. Dent. Res. 63, 618–621. https://doi.org/10.1177/00220345840630050201

Laude, H., 1981. Thermal inactivation studies of a coronavirus, transmissible gastroenteritis

virus. J. Gen. Virol. 56. https://doi.org/10.1099/0022-1317-56-2-235

Leclercq, I., Batéjat, C., Burguière, A.M., Manuguerra, J.C., 2014. Heat inactivation of the Middle East respiratory syndrome coronavirus. Influenza Other Respi. Viruses. https://doi.org/10.1111/irv.12261

Liao, D.L., Xiao, W., Yu, X., Wang, H., Zhao, D.M., Wang, D.Q., 2020. Can N95 facial masks be used after disinfection? And for how many times? ACS Nano 14, 6348–6356. https://doi.org/10.1021/acsnano.0c03597

Lin, K., Marr, L.C., 2020. Humidity-Dependent Decay of Viruses, but Not Bacteria, in Aerosols and Droplets Follows Disinfection Kinetics. Environ. Sci. Technol. 54, 1024–1032. https://doi.org/10.1021/acs.est.9b04959

Mahase, E., 2021. Delta variant: What is happening with transmission, hospital admissions, and restrictions? BMJ 373, 1–2. https://doi.org/10.1136/bmj.n1513

Morris, D.H., Claude Yinda, K., Gamble, A., Rossine, F.W., Bushmaker, T., Fischer, R.J., Jeremiah Matson, M., van Doremalen, N., Vikesland, P.J., Marr, L.C., Munster, V.J., Lloyd-Smith, J.O., 2020. Mechanistic theory predicts the effects of temperature and humidity on inactivation of SARS-CoV-2 and other enveloped viruses. bioRxiv. https://doi.org/10.1101/2020.10.16.341883

Oh, C., Araud, E., Puthussery, J. V., Bai, H., Clark, G.G., Wang, L., Verma, V., Nguyen, T.H., 2020. Dry heat as a decontamination method for n95 respirator reuse. Environ. Sci. Technol. Lett. 7, 677–682. https://doi.org/10.1021/acs.estlett.0c00534

Oral, E., Wannomae, K.K., Connolly, R., Gardecki, J., Leung, H.M., Muratoglu, O., Griffiths, A., Honko, A.N., Avena, L.E., Mckay, L.G.A., Flynn, N., Storm, N., Downs, S.N., Jones, R., Emmal, B., 2020. Vapor H 2 O 2 sterilization as a decontamination method for the reuse

of N95 respirators in the COVID-19 emergency 4, 1–5. https://doi.org/10.1101/2020.04.11.20062026

Paul, R., Das, S.N., Dalui, S., Gayen, R.N., Roy, R.K., Bhar, R., Pal, A.K., 2008. Synthesis of DLC films with different sp2/sp3 ratios and their hydrophobic behaviour. J. Phys. D. Appl. Phys. 41. https://doi.org/10.1088/0022-3727/41/5/055309

Qiao, B., De La Cruz, M.O., 2020. Enhanced binding of SARS-CoV-2 spike protein to receptor by distal polybasic cleavage sites. ACS Nano 14, 10616–10623. https://doi.org/10.1021/acsnano.0c04798

Raeiszadeh, M., Adeli, B., 2020. A Critical Review on Ultraviolet Disinfection Systems against COVID-19 Outbreak: Applicability, Validation, and Safety Considerations. ACS Photonics 7, 2941–2951. https://doi.org/10.1021/acsphotonics.0c01245

Reed, L.J., Muench, H., 1938. A simple method of estimating fifty per cent endpoints. Am. J. Epidemiol. 27, 493–497. https://doi.org/10.1093/oxfordjournals.aje.a118408

Roduner, E., 2014. Understanding catalysis. Chem. Soc. Rev. 43, 8226–8239. https://doi.org/10.1039/c4cs00210e

Rowan, N.J., Laffey, J.G., 2020. Challenges and solutions for addressing critical shortage of supply chain for personal and protective equipment (PPE) arising from Coronavirus disease (COVID19) pandemic – Case study from the Republic of Ireland. Sci. Total Environ. 725, 138532. https://doi.org/10.1016/j.scitotenv.2020.138532

Samarasekera, U., 2021. India grapples with second wave of COVID-19. The Lancet Microbe 2, e238. https://doi.org/10.1016/s2666-5247(21)00123-3

Sanche, S., Lin, Y.T., Xu, C., Romero-Severson, E., Hengartner, N., Ke, R., 2020. High Contagiousness and Rapid Spread of Severe Acute Respiratory Syndrome Coronavirus 2.

Emerg. Infect. Dis. 26, 1470–1477. https://doi.org/10.3201/eid2607.200282

Schipper, R.G., Silletti, E., Vingerhoeds, M.H., 2007. Saliva as research material: biochemical, physicochemical and practical aspects. Arch Oral Biol 52, 1114–1135. https://doi.org/10.1016/j.archoralbio.2007.06.009

Song, C., Havlin, S., 2005. Self-similarity of complex networks 433, 392–395. https://doi.org/10.1038/nature03248

Tao, X., Garron, T., Agrawal, A.S., Algaissi, A., Peng, B.-H., Wakamiya, M., Chan, T.-S., Lu, L., Du, L., Jiang, S., Couch, R.B., Tseng, C.-T.K., 2015. Characterization and Demonstration of the Value of a Lethal Mouse Model of Middle East Respiratory Syndrome Coronavirus Infection and Disease. J. Virol. 90, 57–67. https://doi.org/10.1128/JVI.02009-15

van Doremalen, N., Bushmaker, T., Morris, D.H., Holbrook, M.G., Gamble, A., Williamson, B.N., Tamin, A., Harcourt, J.L., Thornburg, N.J., Gerber, S.I., Lloyd-Smith, J.O., de Wit, E., Munster, V.J., 2020. Aerosol and Surface Stability of SARS-CoV-2 as Compared with SARS-CoV-1. N. Engl. J. Med. https://doi.org/10.1056/NEJMc2004973

van Doremalen, N., Bushmaker, T., Munster, V.J., 2013. Stability of middle east respiratory syndrome coronavirus (MERS-CoV) under different environmental conditions. Eurosurveillance 18, 1–4. https://doi.org/10.2807/1560-7917.ES2013.18.38.20590

Viscusi, D.J., Bergman, M.S., Eimer, B.C., Shaffer, R.E., 2009. Evaluation of five decontamination methods for filtering facepiece respirators. Ann. Occup. Hyg. 53, 815–827. https://doi.org/10.1093/annhyg/mep070

Viscusi, D.J., King, W.P., Shaffer, R.E., 2007. Effect of Decontamination on the Filtration Efficiency of Two Filtering Facepiece Respirator Models. J. Int. Soc. Respir. Prot. 24.

Woo, M.-H., Hsu, Y.-M., Wu, C.-Y., Heimbuch, B., Wander, J., 2010. Method for contamination of filtering facepiece respirators by deposition of MS2 viral aerosols. J. Aerosol Sci. 41, 944–952. https://doi.org/10.1016/j.jaerosci.2010.07.003

Xiang, Y., Song, Q., Gu, W., 2020. Decontamination of surgical face masks and N95 respirators by dry heat pasteurization for one hour at 70°C. Am. J. Infect. Control 48, 880–882. https://doi.org/10.1016/j.ajic.2020.05.026

Yap, T.F., Decker, C.J., Preston, D.J., 2021. Effect of daily temperature fluctuations on virus lifetime. Sci. Total Environ. 789, 148004. https://doi.org/10.1016/j.scitotenv.2021.148004

Yap, T.F., Liu, Z., Shveda, R.A., Preston, D.J., 2020. A predictive model of the temperature-dependent inactivation of coronaviruses. Appl. Phys. Lett. 117. https://doi.org/10.1063/5.0020782

Zha, M., Alsarraj, J., Bunch, B., Venzon, D., 2021. Impact on the fitness of N95 masks with extended use/limited reuse and dry heat decontamination. J. Investig. Med. jim-2021-001908. https://doi.org/10.1136/jim-2021-001908

Zhu, Y., Chen, Y.Q., 2020. On a Statistical Transmission Model in Analysis of the Early Phase of COVID-19 Outbreak. Stat. Biosci. 13, 1–17. https://doi.org/10.1007/s12561-020-09277-0

Zhu, Z., Lian, X., Su, X., Wu, W., Marraro, G.A., Zeng, Y., 2020. From SARS and MERS to COVID-19: A brief summary and comparison of severe acute respiratory infections caused by three highly pathogenic human coronaviruses. Respir. Res. 21, 1–14. https://doi.org/10.1186/s12931-020-01479-w

Appendix A: Supplementary Material

Efficacy and Self-Similarity of SARS-CoV-2 Thermal Decontamination

Te Faye Yap[1,†], Jason C. Hsu[2,†], Zhen Liu[1], Kempaiah Rayavara[2], Vivian Tat[2], Chien-Te K. Tseng[2,3], and Daniel J. Preston[1,*]

[1]Department of Mechanical Engineering, George R. Brown School of Engineering, Rice University; 6100 Main St., Houston, TX 77005, USA.

[2]Department of Microbiology and Immunology, University of Texas Medical Branch; 301 University Blvd., Galveston, TX 77555, USA.

[3]Center for Biodefense and Emerging Disease, Galveston National Laboratory, University of Texas Medical Branch; 301 University Blvd., Galveston, TX 77555, USA.

[†]These authors contributed equally to this work

*Corresponding author. Email: djp@rice.edu

Supplementary Text

1. Statistical Analysis

1.1 Experimental Error Analysis

The experimental error for the concentration measurement at a given temperature can be determined from the standard deviation:

$$\sigma_{[C]} = \sqrt{\frac{1}{N-1}\sum_{i=1}^{N}\left([C_i] - [\overline{C}]\right)^2} \quad \text{[Eq. S1]}$$

where N is the number of data points, $[C_i]$ is the experimental concentration, and $[\overline{C}]$ is the mean concentration for a given time point. To determine the corresponding error in the nondimensionalized concentration, $[C]^*$, the error is propagated based on the method of first partial derivatives:

$$\sigma_{[C]^*} = \sqrt{\left(\frac{\sigma_{[C]}}{[C_0]}\right)^2 + \left(\frac{[C]\cdot\sigma_{[C_0]}}{[C_0]^2}\right)^2} \quad \text{[Eq. S2]}$$

where σ represents the error associated with each measured quantity. This approach is used to determine the combined nondimensionalized error plotted in Figure 2. Error bars plotted on the nondimensionalized logarithmic plot (Figure 1B and 2A) were determined by propagating the error for the log base 10 of $[C]^*$ using the error determined from Eq. S2, shown here in Eq. S3:

$$\sigma_{\log_{10}[C]^*} = \log_{10} e \left(\frac{\sigma_{[C]^*}}{[C]^*}\right) \quad \text{[Eq. S3]}$$

1.2 Identification of Outliers

We nondimensionalized the experimental data from our work and prior work for SARS-CoV-2, SARS-CoV-1, and MERS-CoV, and plotted the data against our universal model in Figure 2 in the main text. To identify outlier points that deviate from the universal model, we evaluate the residuals, ε, of each experimental data point by taking the difference between the experimentally determined y-value (i.e., $\log_{10}[C]^*$) and the model y-value as shown in Eq. S4:

$$y - y_{model} = \varepsilon \quad \text{[Eq. S4]}$$

We determine the sum of squares for the error, SSE, using Eq. S5:

$$\sum_{i=1}^{n} \varepsilon^2 = SSE \quad \text{[Eq. S5]}$$

which is used to determine the standard deviation of the residuals, σ, for each virus dataset:

$$\sigma = \sqrt{\frac{SSE}{n-2}} \quad \text{[Eq. S6]}$$

Data points with residual magnitudes, |ε|, that are positive or greater than two times the standard deviation of the residuals, 2σ, are considered to be outlier data points (Illowsky and Dean, 2021). The two points indicated with arrows in Figure 2(B and D) have residuals greater than 2σ. Tables S1–4 show the values for the statistical parameters used to determine the outliers for each dataset in Figure 2. The outlier data points are bolded and labeled with an asterisk in the tables.

2. Procedure to Determine E_a and ln(A)

2.1. Data Visualization and Interpretation

The experimental data are plotted according to the linearized rate law for a first-order reaction (Eq. S7) as shown in Figure S1. The magnitude of the slope of the best fit line corresponds to the rate constant, k, at a given temperature, T.

$$ln\frac{[C]}{[C_0]} = -kt \quad \text{[Eq. S7]}$$

Each pair of (k, T) is plotted in Figure S2 according to the linearized Arrhenius equation (Eq. S8) and the values are tabulated in Table S5:

$$\ln(k) = -\frac{E_a}{RT} + ln(A) \quad \text{[Eq. S8]}$$

where R is the gas constant, E_a is the activation energy associated with inactivation for a given virus, and A is the frequency factor. The values of E_a and ln(A) for the SARS-CoV-2 virus can be determined by equating $-E_a/R$ and ln(A) to the slope (Eq. S9) and intercept (Eq. S10) of the linear fit with the form of the linearized Arrhenius equation shown in Figure S2, respectively.

$$-\frac{E_a}{R\times 10^4} = slope \quad \text{[Eq. S9]}$$

$$\ln(A) = intercept \quad \text{[Eq. S10]}$$

The linear correlation between E_a and ln(A) for the range of coronaviruses shown in Figure S3 indicates that they undergo a thermal denaturation process following the Meyer-Neldel rule (Qin et al., 2014; Wright, 2003), which arises from entropy-enthalpy compensation. The E_a and ln(A) for SARS-CoV-2 determined in this work are plotted with the values for other coronaviruses determined in prior work; the overlap indicates that the inactivation behavior is similar. The

values of E_a and ln(*A)* for SARS-CoV-2 and the percentage differences between the values determined in this work and in a prior data-driven study (Yap et al., 2020) are tabulated in Table S6.

2.2. Inactivation Rate Model

The rate law for a first-order reaction (Eq. S7) and the Arrhenius equation (Eq. S8) were combined by substituting the Arrhenius equation, rearranged in terms of rate constant, into the expression for the rate law. We rearranged to generate an analytical model for the thermal decontamination time as a function of temperature (Eq. 1 in the main text).

2.3. Linearly-Scaled Experimental Data

The experimental results are plotted with linear axes in Figure S4 to provide an additional view from which to compare the decrease in concentration of viable virions versus time at four different temperatures (as opposed to the log axes used in the main text Figure 1B).

3. Procedure to Determine Relative Humidity at Elevated Temperatures

Relative humidity (RH) is the ratio of actual water vapor pressure or vapor density, ρ_{act}, in the air compared to the saturated vapor pressure or vapor density, $\rho_{sat,T}$, at a given temperature. Because the relative humidity depends on temperature, as we heat the samples in a closed oven with a fixed volume of air, the relative humidity will decrease. Taking the initial conditions of the ambient air temperature to be 25 °C and the relative humidity, $RH_{initial,\ 25\ °C}$ to be 50% (within our reported RH range), we can determine the actual water vapor density in the air using Eq. S11:

$$RH_{intial,25℃} = \frac{Actual\ vapor\ density, \rho_{act}}{Saturated\ vapor\ density\ at\ 25℃, \rho_{sat,25\ ℃}} \quad \text{[Eq. S11]}$$

Rearranging the terms to determine the ρ_{act}:

$$\rho_{act} = 50\% \times \rho_{sat,25℃} \quad \text{[Eq. S12]}$$

The $\rho_{sat,T}$ for a given temperature can be determined from fluid property tables for saturated water (Çengel and Boles, 2015). After the oven heats up to a given setpoint temperature, we can

determine the new relative humidity in the oven at elevated temperatures (Eq. S13) using ρ_{act} determined from Eq. S12.

$$RH_{oven,T} = \frac{\rho_{act}}{Saturated\ vapor\ density\ at\ 25℃, \rho_{sat,70\ ℃}} \quad \text{[Eq. S13]}$$

The values of the parameters and the estimated relative humidity at each oven setpoint temperature are tabulated in Table S7. The estimated relative humidity value at 70 °C is in close agreement with relative humidity measurements of air inside a heated electric cooker measured using a thermo-hygrometer at 100 °C, which were reported as ~ 5% in prior work (Oh et al., 2020).

4. Degradation of Meltblown Filter Layer

Surgical masks were heated to elevated temperatures greater than those used for decontamination in our work, and SEM images were taken to illustrate the changes in physical morphology of heat-degraded meltblown filter layers. Prior work reported a decrease in filtration efficiency when heating the meltblown filter layer to 125 °C (Liao et al., 2020); using SEM imaging, we compare a sample heated to 125 °C (the reported temperature where degradation occurs) for 30 minutes in Figure S5A to an unheated sample in Figure 3B. We observe a change in the physical morphology due to relaxation of the crystalline structure as we increase the temperature close to the polymer's melting point (Campos et al., 2020). The material used in the meltblown filter layer (i.e., polypropylene) has typical melting points ranging from 130 °C to 170 °C. To further demonstrate the sensitivity of the meltblown layer morphology to high temperatures, we heated the filter layer to 150 °C (for 10 minutes), 155 °C (for 2 minutes), and 160 °C (for 2 minutes) and observed a significant change in the physical morphology and degradation of the filter layer (Figure S5B–D). This characterization method shows that typical dry heat decontamination temperatures (~160 °C) are not suitable for decontaminating delicate PPE (Darmady et al., 1961).

5. Transient Heating Period of Samples

We characterized the experimental temperature profile of a mask sample as it heated up in the oven to determine whether the transient heating period represented a significant source of error.

We placed a mask sample on a preheated plate following the same procedure used in all of the experiments, and we recorded the temperature of the mask over time. We determined that the sample heats up to the setpoint temperature in approximately 30 seconds. We show the experimentally measured temperature profile of the mask sample being heat treated at 70 °C in Figure S6. The time required for the mask temperature to reach the setpoint temperature, 70 °C, is ~10 % of the total time required to achieve a 3-log reduction of SARS-CoV-2 (5 minutes), which is the shortest decontamination duration studied in our work. For longer decontamination times and at lower temperatures, the percentage of the total time for the transient heating period is smaller, and it does not represent a significant source of error in any of our experiments.

Supplementary Figures

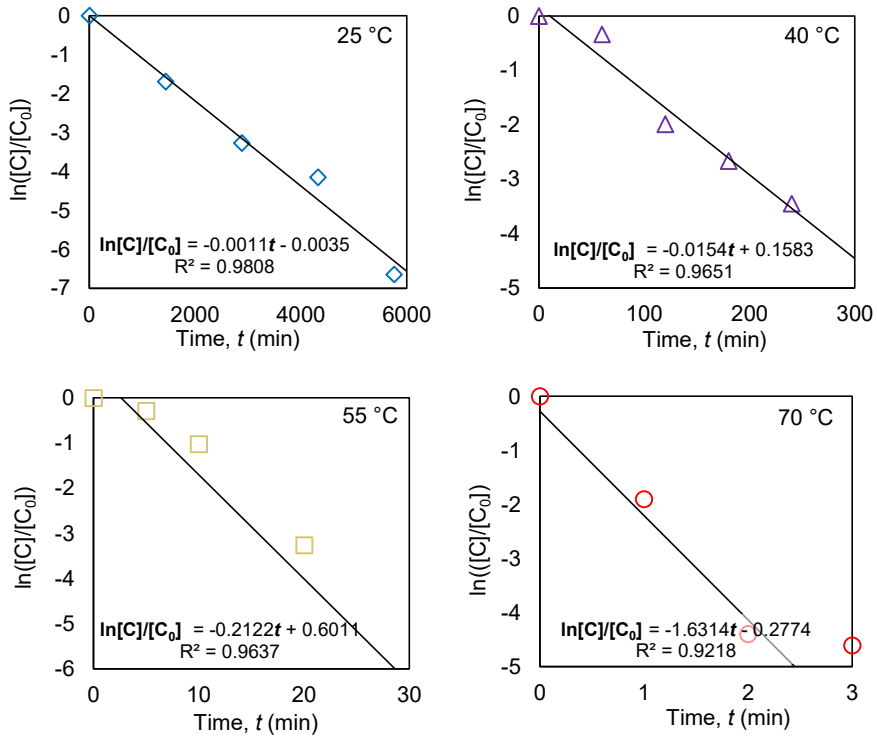

Figure S1. Primary data for inactivation of SARS-CoV-2 on surgical masks after converting the n-log reduction values from log base 10 to natural log. We fit a line according to Eq. S7 to the data to estimate the rate constants at 25 °C, 40 °C, 55 °C, and 70 °C.

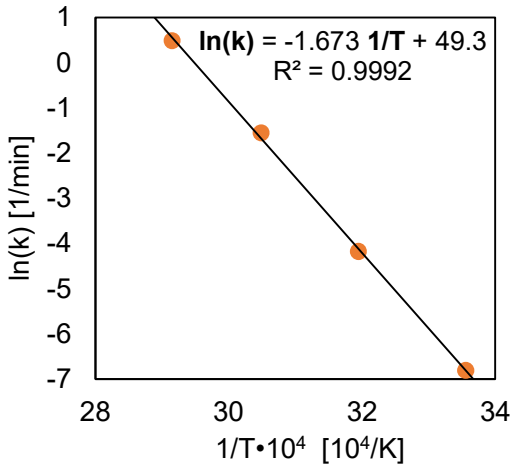

Figure S2. From the primary data, the rate constant, k, for a given temperature was determined using a linear regression according to Eq. S8. The slope and intercept of the linear fit correspond to the activation energy, E_a, and frequency factor, ln(A), for SARS-CoV-2.

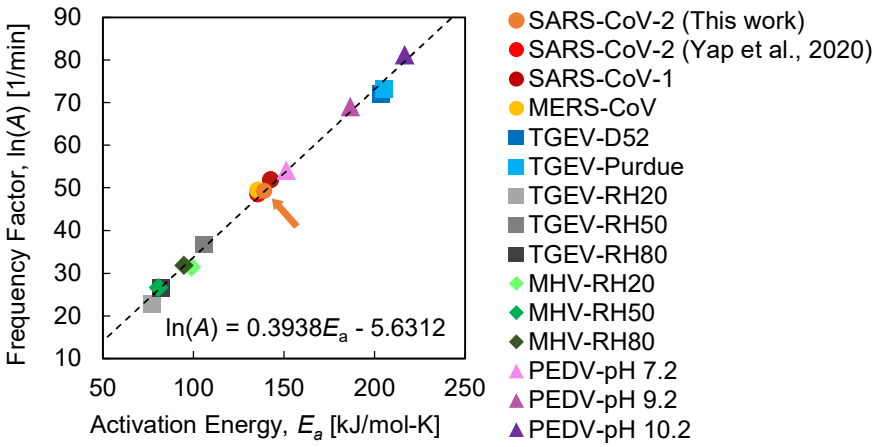

Figure S3. Thermal inactivation behavior of a range of coronaviruses, adapted from prior work (Yap et al., 2020) that applied a data-driven approach. The frequency factor, ln(A), is plotted against the activation energy, E_a, according to the Arrhenius equation; the linear relationship indicates protein denaturation. The E_a and ln(A) determined in this work (indicated by the arrow) are similar to the values determined in prior work for SARS-CoV-2 on a range of fomites.

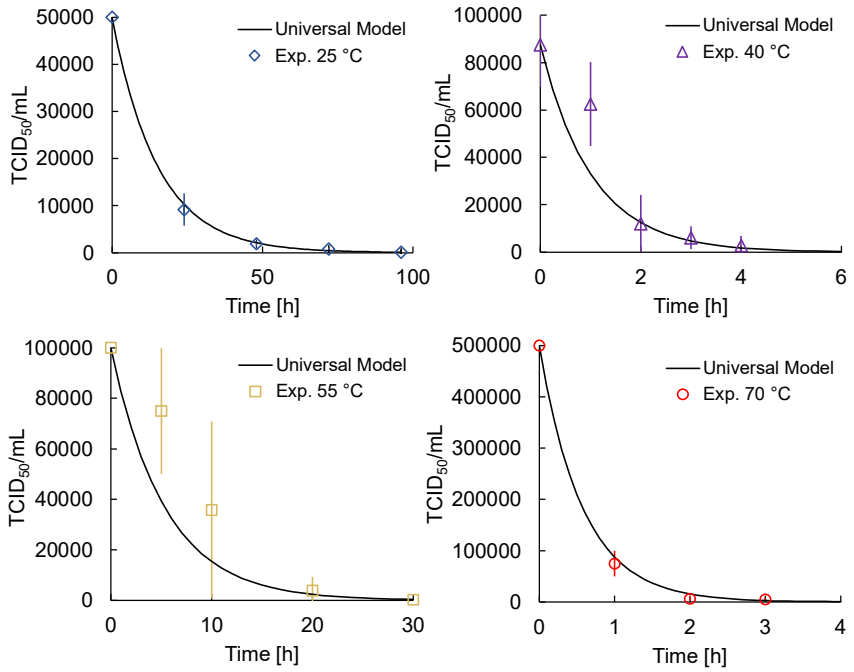

Figure S4. Experimental results obtained at 25 °C, 40 °C, 55 °C, and 70 °C show that the inactivation timescale for decontamination of SARS-CoV-2 on PPE spans more than three orders of magnitude (i.e., from less than 5 minutes to nearly 100 hours for a 3-log reduction corresponding to effective decontamination).

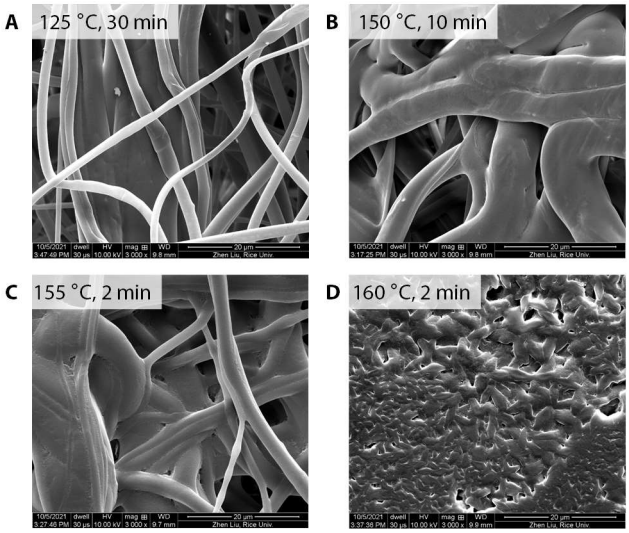

Figure S5. SEM images of the meltblown filter layer after dry heat treatment at (A) 125 °C for 30 minutes, (B) 150 °C for 10 minutes, (C) 155 °C for 2 minutes, and (D) 160 °C for 2 minutes.

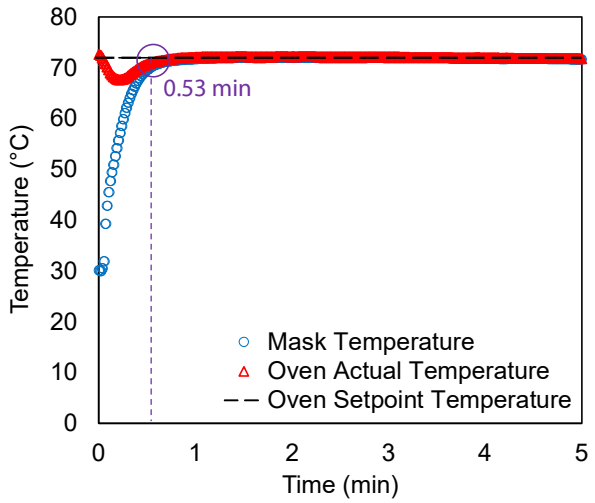

Figure S6. Temperature profile of a mask sample heated to 70 °C. The actual temperature in the oven dipped below the setpoint when the door of the oven was opened to load the sample, but the temperature quickly returned to the setpoint temperature after the door was closed. The mask sample temperature increased from room temperature initially (time = 0 min) to the oven setpoint in less than one minute.

Table S1. Statistical parameters used in determining the outliers for SARS-CoV-2 inactivation in this work.

T(°C)	t^*	$\log(C^*)_{exp.}$	$\varepsilon = \log(C^*)_{exp} - \log(C^*)_{model}$	ε^2	$\lvert \varepsilon \rvert - 2\sigma$
25	0	0	0.000	0.000	-0.445
25	0.708	- 0.737	-0.028	0.001	-0.417
25	1.417	- 1.420	-0.003	0.000	-0.441
25	2.125	- 1.800	0.325	0.106	-0.120
25	2.834	- 2.886	-0.052	0.003	-0.393
40	0	0	0.000	0.000	-0.445
40	0.434	- 0.146	0.288	0.083	-0.157
40	0.868	- 0.863	0.005	0.000	-0.440
40	1.302	-1.158	0.144	0.021	-0.301
40	1.736	-1.499	0.237	0.056	-0.208
55	0	0	0.000	0.000	-0.445
55	0.416	-0.125	0.291	0.085	-0.154
55	0.832	-0.446	0.386	0.149	-0.059
55	1.663	-1.416	0.247	0.061	-0.198
55	2.500	-2.699	-0.204	0.042	-0.241
70	0	0	0.000	0.000	-0.445
70	0.772	-0.824	-0.051	0.003	-0.393
70	1.545	-1.909	-0.364	0.132	-0.081
70	2.317	-2	0.317	0.101	-0.127
				SSE = 0.841	σ = 0.222

Table S2. Statistical parameters used in determining the outliers for SARS-CoV-2 inactivation in prior work (Chin et al., 2020; van Doremalen et al., 2020).

T(°C)	t^*	$\log(C^*)_{exp.}$	$\varepsilon = \log(C^*)_{exp} - \log(C^*)_{model}$	ε^2	$\lvert \varepsilon \rvert - 2\sigma$
20	0	0	0	0	-1.241
20	0.022	-0.420	-0.398	0.159	-0.843
20	0.087	-0.440	-0.353	0.124	-0.888
20	0.174	-0.590	-0.416	0.173	-0.825
20	0.523	-1.110	-0.587	0.344	-0.654
20	**1.047**	**-2.330**	**-1.283**	**1.647**	**0.043***
22	0	0	0	0	-1.241
22	0.008	-0.030	-0.022	0.000	-1.219
22	0.050	-0.670	-0.620	0.384	-0.621
22	0.100	-0.810	-0.710	0.504	-0.531
22	0.400	-1.050	-0.650	0.422	-0.591
22	0.801	-1.580	-0.779	0.607	-0.462
22	1.602	-2.070	-0.468	0.219	-0.773
22	2.803	-2.990	-0.187	0.035	-1.054
				SSE = 4.619	σ = 0.620

Table S3. Statistical parameters used in determining the outliers for SARS-CoV-1 inactivation in prior work (Darnell and Taylor, 2006; van Doremalen et al., 2020).

T(°C)	t^*	$\log(C^*)_{exp.}$	$\varepsilon = \log(C^*)_{exp} - \log(C^*)_{model}$	ε^2	$\lvert \varepsilon \rvert - 2\sigma$
22	0	0	0	0	-0.545
22	0.051	-0.390	-0.339	0.115	-0.206
22	0.203	-0.320	-0.117	0.014	-0.429
22	0.407	-0.760	-0.353	0.125	-0.192
22	1.220	-1.480	-0.260	0.068	-0.285
22	2.440	-2.540	-0.100	0.010	-0.445
56	0	0	0	0	-0.545
56	3.462	-3.959	-0.497	0.247	-0.049
65	0	0	0.000	0	-0.545
65	1.336	-1.205	0.131	0.017	-0.414
				SSE = 0.595	σ = 0.273

Table S4. Statistical parameters used in determining the outliers for MERS-CoV inactivation in this work (Leclercq et al., 2014; van Doremalen et al., 2013).

T(°C)	t^*	$\log(C^*)_{exp.}$	$\varepsilon = \log(C^*)_{exp} - \log(C^*)_{model}$	ε^2	$\lvert \varepsilon \rvert - 2\sigma$
20	0.000	0.000	0.000	0.000	-1.311
20	0.010	0.132	0.142	0.020	-1.169
20	0.029	-0.538	-0.509	0.259	-0.802
20	0.235	-0.560	-0.325	0.105	-0.986
20	0.471	-1.021	-0.551	0.303	-0.760
20	1.412	-1.416	-0.004	0.000	-1.307
20	**2.824**	**-4.326**	**-1.502**	**2.256**	**0.191***
20	4.236	-4.714	-0.478	0.229	-0.833
56	0.000	0.000	0.000	0.000	-1.311
56	0.214	-0.090	0.124	0.015	-1.186
56	0.214	0.580	0.794	0.631	-0.516
56	0.214	-0.920	-0.706	0.498	-0.605
65	0.000	0.000	0.000	0.000	-1.311
65	0.801	-0.920	-0.119	0.014	-1.192
65	0.801	-1.920	-1.119	1.252	-0.192
				SSE = 5.582	σ = 0.655

Table S5. The rate constant, *k*, at each experimental temperature determined from Figure S1 and plotted in Figure S2.

Temperature [°C]	$1/T \bullet 10^4$ [10^4/K]	*k* [1/min]	ln(*k*)
25	33.56	0.0011	- 6.812
40	31.95	0.0154	- 4.173
55	30.49	0.2122	-1.550
70	29.15	1.6314	0.489

Table S6. The frequency factor, ln(A), and activation energy, E_a, for SARS-CoV-2 determined from the present experimental work and from a data-driven approach used in prior work (Yap et al., 2020).

	Frequency factor, ln(A) [1/min]	Activation energy, E_a [kJ/mol]
Present work	49.3	139.1
Prior data-driven approach (Yap et al., 2020)	48.6	135.7
Percent difference (%)	1.46	2.48

Table S7. Values used to estimate the relative humidity at different oven setpoint temperatures.

T (°C)	$\rho_{sat.\,T}$ (kg/m^3)	RH (%).
25	0.0231	50
40	0.0512	23
55	0.1045	11
70	0.1984	6

Supplementary References

Campos, R.K., Jin, J., Rafael, G.H., Zhao, M., Liao, L., Simmons, G., Chu, S., Weaver, S.C., Chiu, W., Cui, Y., 2020. Decontamination of SARS-CoV-2 and other RNA viruses from N95 level meltblown polypropylene fabric using heat under different humidities. ACS Nano 14, 14017−14025. https://doi.org/10.1021/acsnano.0c06565

Çengel, Y. a., Boles, M.A., 2015. Thermodynamics: An Engineering Approach, 8th ed, McGraw-Hill. McGraw Hill Education.

Chin, A.W.H., Chu, J.T.S., Perera, M.R.A., Hui, K.P.Y., Yen, H.-L., Chan, M.C.W., Peiris, M., Poon, L.L.M., 2020. Stability of SARS-CoV-2 in different environmental conditions. The Lancet Microbe 1, e10. https://doi.org/10.1016/S2666-5247(20)30003-3

Darmady, E.M., Hughes, K.E., Jones, J.D., Prince, D., Tuke, W., 1961. Sterilization by dry heat. J. Clin. Pathol. 14, 38–44. https://doi.org/10.1136/jcp.14.1.38

Darnell, M.E.R., Taylor, D.R., 2006. Evaluation of inactivation methods for severe acute respiratory syndrome coronavirus in noncellular blood products. Transfusion 46, 1770–1777. https://doi.org/10.1111/j.1537-2995.2006.00976.x

Illowsky, B., Dean, S., 2021. Outliers [WWW Document]. URL https://stats.libretexts.org/@go/page/802 (accessed 10.7.21).

Leclercq, I., Batéjat, C., Burguière, A.M., Manuguerra, J.C., 2014. Heat inactivation of the Middle East respiratory syndrome coronavirus. Influenza Other Respi. Viruses. https://doi.org/10.1111/irv.12261

Liao, L., Xiao, W., Zhao, M., Yu, X., Wang, H., Wang, Q., Chu, S., Cui, Y., 2020. Can N95 respirators be reused after disinfection? And for how many times? ACS Nano 14, 6348–6356. https://doi.org/10.1021/acsnano.0c03597

Oh, C., Araud, E., Puthussery, J. V., Bai, H., Clark, G.G., Wang, L., Verma, V., Nguyen, T.H., 2020. Dry heat as a decontamination method for n95 respirator reuse. Environ. Sci. Technol. Lett. 7, 677–682. https://doi.org/10.1021/acs.estlett.0c00534

Qin, Z., Balasubramanian, S.K., Wolkers, W.F., Pearce, J.A., Bischof, J.C., 2014. Correlated Parameter Fit of Arrhenius Model for Thermal Denaturation of Proteins and Cells. Ann. Biomed. Eng. https://doi.org/10.1007/s10439-014-1100-y

van Doremalen, N., Bushmaker, T., Morris, D.H., Holbrook, M.G., Gamble, A., Williamson, B.N., Tamin, A., Harcourt, J.L., Thornburg, N.J., Gerber, S.I., Lloyd-Smith, J.O., de Wit, E., Munster, V.J., 2020. Aerosol and Surface Stability of SARS-CoV-2 as Compared with SARS-CoV-1. N. Engl. J. Med. https://doi.org/10.1056/NEJMc2004973

van Doremalen, N., Bushmaker, T., Munster, V.J., 2013. Stability of middle east respiratory syndrome coronavirus (MERS-CoV) under different environmental conditions. Eurosurveillance 18, 1–4. https://doi.org/10.2807/1560-7917.ES2013.18.38.20590

Wright, N.T., 2003. On a relationship between the Arrhenius parameters from thermal damage studies. J. Biomech. Eng. 125, 300–304. https://doi.org/10.1115/1.1553974

Yap, T.F., Liu, Z., Shveda, R.A., Preston, D.J., 2020. A predictive model of the temperature-dependent inactivation of coronaviruses. Appl. Phys. Lett. 117. https://doi.org/10.1063/5.0020782